Opto-Electronic Advances

ISSN 2096-4579 CN 51-1781/TN

Paving continuous heat dissipation pathways for quantum dots in polymer with orange-inspired radially aligned UHMWPE fibers

Xuan Yang, Xinfeng Zhang, Tianxu Zhang, Linyi Xiang, Bin Xie and Xiaobing Luo

Citation: Yang X, Zhang XF, Zhang TX, et al. Paving continuous heat dissipation pathways for quantum dots in polymer with orange-inspired radially aligned UHMWPE fibers. *Opto-Electron Adv* **7**, 240036(2024).

https://doi.org/10.29026/oea.2024.240036

Received: 20 February 2024; Accepted: 11 May 2024; Published online: 5 July 2024

Opto-Electronic Advances

Article

July 2024, Vol. 7, No. 7

DOI: 10.29026/oea.2024.240036

Paving continuous heat dissipation pathways for quantum dots in polymer with orange-inspired radially aligned UHMWPE fibers

Xuan Yang[1], Xinfeng Zhang[1], Tianxu Zhang[1], Linyi Xiang[1], Bin Xie[2]* and Xiaobing Luo[1]*

Thermal management of nanoscale quantum dots (QDs) in light-emitting devices is a long-lasting challenge. The existing heat transfer reinforcement solutions for QDs-polymer composite mainly rely on thermal-conductive fillers. However, this strategy failed to deliver the QDs' heat generation across a long distance, and the accumulated heat still causes considerable temperature rise of QDs-polymer composite, which eventually menaces the performance and reliability of light-emitting devices. Inspired by the radially aligned fruit fibers in oranges, we proposed to eliminate this heat dissipation challenge by establishing long-range ordered heat transfer pathways within the QDs-polymer composite. Ultrahigh molecular weight polyethylene fibers (UPEF) were radially aligned throughout the polymer matrix, thus facilitating massive efficient heat dissipation of the QDs. Under a UPEF filling fraction of 24.46 vol%, the in-plane thermal conductivity of QDs-radially aligned UPEF composite (QDs-RAPE) could reach 10.45 W m^{-1} K^{-1}, which is the highest value of QDs-polymer composite reported so far. As a proof of concept, the QDs' working temperature can be reduced by 342.5 °C when illuminated by a highly concentrated laser diode (LD) under driving current of 1000 mA, thus improving their optical performance. This work may pave a new way for next generation high-power QDs lighting applications.

Keywords: quantum dots; UHMWPE fibers; radial alignment; heat dissipation; light-emitting devices

Yang X, Zhang XF, Zhang TX et al. Paving continuous heat dissipation pathways for quantum dots in polymer with orange-inspired radially aligned UHMWPE fibers. *Opto-Electron Adv* **7**, 240036 (2024).

Introduction

Recently, three scientists shared the 2023 Nobel Prize in Chemistry for their discovery and synthesis of quantum dots (QDs), a kind of luminescent nanocrystals featuring tunable band gap, wide light absorption spectrum, high quantum yield (QY) and superior color purity[1–4]. These remarkable properties make QDs widely adopted in optoelectronic fields such as solar cells[5–7], photodetectors[8–10], light-emitting diodes (LEDs)[11,12], and laser diodes (LDs)[13,14]. During the photoluminescence process of QDs, both light conversion and heat generation happen simultaneously. For the light conversion process, when electron transits between the discrete energy levels, it releases energy by emitting photons as radiative process. For the heat generation process, the released energy is converted into thermal phonons as non-radiative process which generates heat and leads to a temperature rise[15,16]. However, QDs are usually embedded in polymer matrix with extremely low thermal conductivity (lower than 0.2 W m^{-1} K^{-1}), which severely

[1]School of Energy and Power Engineering, Huazhong University of Science and Technology, Wuhan 430074, China; [2]School of Mechanical Science and Engineering, Huazhong University of Science and Technology, Wuhan 430074, China.

*Correspondence: B Xie, E-mail: binxie@hust.edu.cn; XB Luo, E-mail: luoxb@hust.edu.cn

Received: 20 February 2024; Accepted: 11 May 2024; Published online: 5 July 2024

hinders the heat generated by QDs from dissipating outward. As a result, the working temperature of the composites reaches to a high level (> 130 °C)[17,18]. Unfortunately, QDs are sensitive to ambient temperature. High temperature could irreversibly damage the structure of QDs and detach the surface ligands to form trap states, causing significant luminescence decline and even thermal quenching[19–22]. Thus, maintaining low QDs' temperature is essential for the applications of QDs in light-emitting devices[23,24].

To tackle the thermal issues in QDs-polymer composites, several strategies have been developed. The most frequently used method is embedding QDs into, or coating QDs with highly thermal-conductive matrix[25,26]. However, the optical performances of the light-emitting devices were worsened since the QDs were damaged by the complicated fabrication process. Alternatively, incorporating highly thermal-conductive fillers with neglectable absorption of visible light (such as hexagonal boron nitride, hBN) into the luminescent composites of silicone-based matrix is available. The loading fraction of the fillers were usually low to enhance the heat dissipation and maintain optical performances simultaneously[20,27–32]. Nevertheless, considerable interfacial thermal resistance between the micro-scale fillers and between the fillers and matrix would make it inefficient to dissipate heat[33], which cannot fulfill the thermal management requirement in high-power density circumstances, such as in white laser diodes (WLDs). To efficiently protect QDs from high temperature, it is urgently needed to constructing continuous heat dissipation channels with low interfacial thermal resistance.

Oranges contain massive radially aligned fruit fibers which offers efficient pathways for transmission of water, as shown in Fig. 1(a). Through radially aligned fruit fibers, the water absorbed from environment can be efficiently delivered from center to the whole orange. Inspired by these fruit fiber networks, we proposed a QDs-radially aligned UPEF composite (QDs-RAPE) by constructing radially-aligned thermal-conductive networks in QDs luminescent composites (QDs-LC), by using ultrahigh molecular weight polyethylene fibers (UHMW-PE fibers, UPEF) with high thermal conductivity ~60 W m^{-1} K^{-1} [34,35]. The meter-scale length of UPEF endows them with continuous and long-range heat dissipation pathways that considerably reduces the interfacial thermal resistance. The QDs-RAPE achieved an in-plane thermal conductivity as high as 10.45 W m^{-1} K^{-1} under UPEF volume ratio of 24.46%, which is the highest value of QDs-polymer composites reported so far. Its excellent thermal conduction ability in the in-plane direction could uniformly conduct the concentrated heat to the whole composites and significantly decrease the temperature. When excited by a blue LD under driving current of 1000 mA, the QDs-RAPE with different UPEF volume ratio realized a huge temperature reduction over 342.5 °C compared with traditional QDs-LC. Contributed by the sharp temperature reduction, the QDs-RAPE could operate stably under higher driving currents (1500 mA), while the QDs-LC suffered from thermal quenching when the driving current exceeded 1000 mA. Moreover, it is proved that with proper volume ratio of UPEF, QDs-RAPE exhibited superior optical performances (luminous efficiency (LE) of 155.85 lm W^{-1} and color rendering index (CRI) of 87.9 at 700 mA) when compared with QDs-LC (LE of 134.04 lm W^{-1} and CRI of 84.2 at 700 mA), especially under high driving currents. This work provides a promising strategy for solving the thermal management challenge of QDs without sacrificing their optical performances, which may pave a new way for next generation high-power QDs lighting applications.

Experimental section

Materials

UPEF with an average diameter of 20 μm were provided by Dongguan Sovetl Special Rope & Webbing Co., Ltd (China), as shown in Fig. S1. Red-emissive CdSe/ZnS QDs-chloroform solution (20 mg/mL) with a peak wavelength of 630 nm were provided by Poly Opto-Electronics (China). Yellow-emissive YAG:Ce phosphor with a peak wavelength of 538 nm were purchased from Intematix. Two-component silicone was purchased from Dowsil (SYLGARD 184, A:B = 10:1).

Fabrication of radially aligned UPEF-silicone composites

A cylindrical template with a diameter of 25 mm was used to fabricated radially aligned UPEF-silicone composites (RA-PE) with different UPEF volume fraction (3.34, 8.22, 12.46, 18.11, 22.57 and 24.46 vol%). First, UPEF were evenly winded along radial direction on the upper surface of the cylindrical template to form radial networks. Then, silicone gel was poured into the radial UPEF networks, and vacuum was applied to let the

silicone gel fully infiltrate the network, followed by a thermal-curing process of 85 °C for 25 minutes. Finally, extra UPEF on the other sides of the template were cut off and the fabricated RA-PE was removed from the template.

Fabrication of QDs-LC and QDs-RAPE

At first, 2 g silicone gel, 0.4 g phosphor and 130 μL QDs-chloroform solution were uniformed mixed and well vacuumed to prepare the QDs-phosphor gel. To fabricated QDs-LC, 0.5 g QDs-phosphor gel was poured into a circular mold with a diameter of 25 mm and then thermal cured for 25 minutes. For QDs-RAPE with different UPEF volume fraction (8.15, 11.93, 17.70, 21.92 and 26.70 vol%), the fabrication process was similar with that of RA-PE. 0.5 g mixed gel were poured into the prepared radially aligned UPEF networks and vacuumed, followed by a thermal-curing process of 85 °C for 25 minutes, as illustrated in Fig. 1.

Characterizations

Scanning electron microscope (SEM) images and energy-dispersive spectroscopy (EDS) mapping images of UPEF and QDs-RAPE were obtained by a field-emission SEM (GeminiSEM300, Carl Zeiss). The ultraviolet-visible (UV-VIS) absorption spectra of the samples were measured by a UV-VIS spectrophotometer (UV-3600, Shimadzu). The photoluminescence (PL) spectra and time resolved PL (TRPL) were carried out by a Fluorescence spectrofluorometer (EI FLS980, Edinburgh Instruments) at a pulse excitation wavelength of 450 nm. The in-plane and through-plane thermal diffusivity α of RA-PE were measured through a laser flash analysis (LFA457, Netzsch). Specific heat capacity of C_p of the samples were obtained by a differential scanning calorimetry (Diamond DSC, PerkinElmer). Density ρ of the samples were tested by an electron density meter (XF-220SD, LICHEN). Thermal conductivity κ of the samples were calculated through $\kappa = \alpha \cdot C_p \cdot \rho$. Optical performances were obtained by an integrating sphere system (ATA-1000, Everfine). Surface temperature distributions of QDs-LC and QDs-RAPE were measured by a thermal infrared imager (SC620, FLIR). The samples were excited by a commercial laser diode (L450P1600MM, Thorlabs).

Results and discussion

Figure 2(a) shows the as-fabricated QDs-RAPE, whose surface presents radial textures formed by UPEF networks. From the optical microscope image in Fig. 2(b), it is observed that UPEF are well-ordered along radial

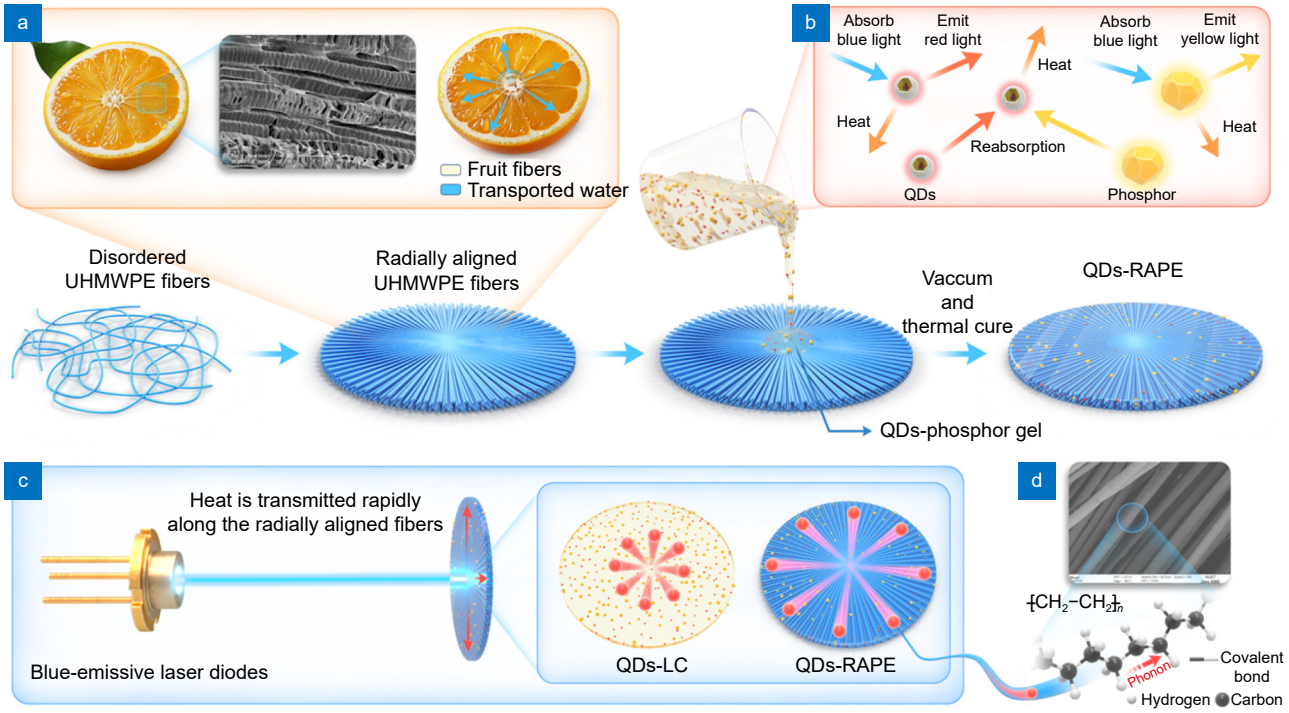

Fig. 1 | Fabrication process of QDs-RAPE. (**a**) SEM image of fruit fibers of oranges and diagram illustration of water transportation with the radially aligned fruit fibers networks. (**b**) Light conversion and heat generation process of QDs and phosphor. (**c**) Schematic of operated transmissive WLDs and comparison of heat dissipation ability of QDs-LC and QDs-RAPE. (**d**) SEM image and schematic of molecular chains of UPEF.

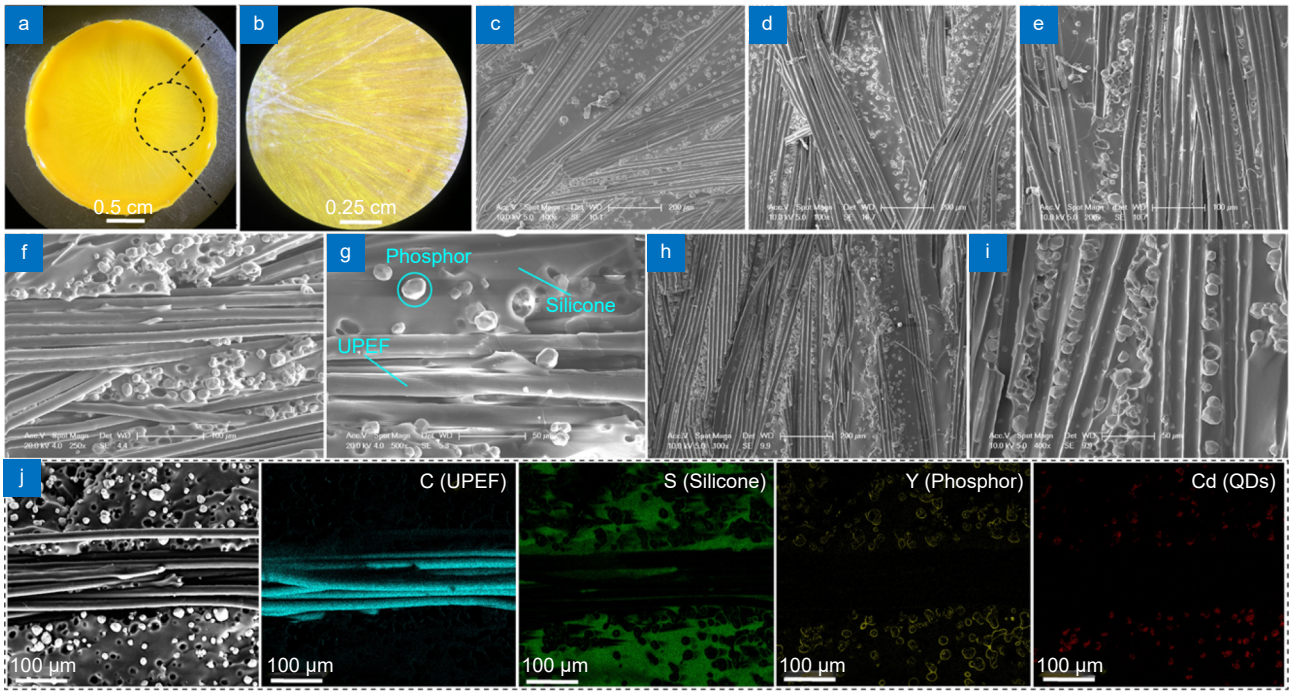

Fig. 2 | (**a**) Photograh of QDs-RAPE. (**b**) Partial enlarged image of QDs-RAPE under optical microscope. (**c–g**) SEM images of QDs-RAPE under different magnifications. (**h–i**) SEM images of QDs-RAPE after removing UPEF under different magnifications. (**j**) SEM image and corresponding EDS mapping images of QDs-RAPE.

directions. SEM images in Fig. 2(c, d) and 2(e) demonstrated that phosphors were uniformly distributed in the silicone matrix and UPEF were embedded in luminescent composites where the continuous columnar UPEF fibers could be observed being paved in the low thermal-conductive matrix. Figure 2(f) and 2(g) show the detailed distribution of the UPEF and phosphor where the QDs were too small to be observed. To clearly exhibited the distribution of the phosphor, the UPEF in QDs-RAPE were removed and it was shown in Fig. 2(h) and 2(i). The images illustrate that phosphor were located closely to the UPEF which offered them with highly thermal-conductive channels. In Fig. 2(j), the EDS mapping images show the distribution of C, Si, Cd and Y elements which confirms that QDs and phosphor are well dispersed around high thermal-conductive UPEF to be efficiently cooled.

Furtherly, to investigate the effect of radially aligned UPEF network on the optical response of QDs and phosphor, UV-VIS absorption spectra and PL spectra of the composites were measured and shown in Fig. 3(a) and 3(b). QDs showed a strong and wide-range absorption in silicone, of which the highest was located at 400 nm, while the light absorption of phosphor in silicone mainly appeared around 300 nm and 450 nm. Additionally, being excited at 450 nm, QDs in silicone displayed a narrow PL spectrum with a peak wavelength of 630 nm and a full-width-at-half-maximum (FWHM) of 32 nm, while phosphor in silicone showed a wider PL spectrum with a peak wavelength of 538 nm and a FWHM of 112 nm. Comparing the absorption and PL spectra of QDs-LC with QDs-RAPE, it is proved that the addition of UPEF networks has little influence on absorption and photoluminescent characteristics contributed by QDs and phosphor. Moreover, PL lifetime of QDs were measured to study their luminous stability in different composites, as shown in Fig. 3(c). These TRPL decay curves were well fitted by an exponential function $I(t) = A_1e^{-t/\tau1} + A_2e^{-t/\tau2}$, where $I(t)$ represents the PL initial intensity at time t. The PL lifetime of QDs in chloroform, silicone and RAPE were calculated as 29.12, 17.71 and 18.43 ns, respectively. The results showed that QDs' PL lifetime in chloroform was higher than those in silicone and silicone with radially aligned UPEF. This is mainly because of the high temperature during the thermal curing process of silicone, which created trap states in QDs and increased the non-radiative process. The little difference on PL lifetime in silicone and silicone with radially aligned UPEF demonstrated that UPEF networks do not affect the luminous stability of QDs.

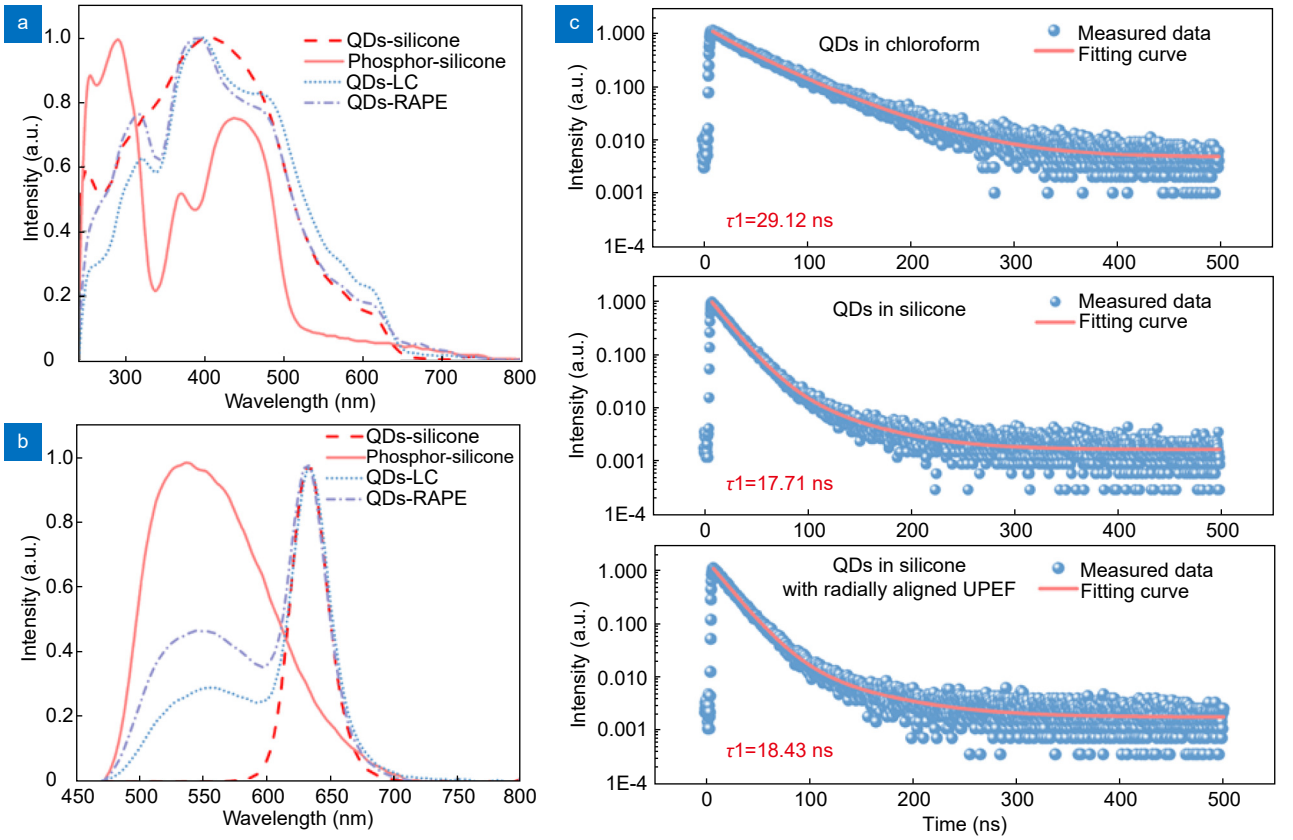

Fig. 3 | (**a**) UV-VIS absorption spectra and (**b**) photoluminescence spectra of QDs-silicone, phosphor-silicone, QDs-LC and QDs-RAPE, respectively. (**c**) TRPL decay curves of QDs in chloroform, silicone and silicone with radially aligned UPEF, respectively.

Figure 4 gives through-plane thermal conductivities (through-plane TC), in-plane thermal conductivities (in-plane TC) and anisotropic degrees of TC of RA-PE with different UPEF volume ratio (3.34, 8.22, 12.46, 18.11, 22.57 and 24.46 vol%), respectively. Owing to the existence of continuous UPEF along the radial direction, in-plane TC of fabricated RA-PE exceeded 1.64 W m^{-1} K^{-1} and reached as high as 10.45 W m^{-1} K^{-1} at 24.46 vol% of UPEF, which were 10.93 and 69.66 times that of pure silicone (0.15 W m^{-1} K^{-1}), respectively. Their through-plane TCs were much lower, which range from 0.19 to 0.46 W m^{-1} K^{-1}. Therefore, the anisotropic degrees of RA-PE were over 20 under higher UPEF volume fraction. In previous studies, hBN was incorporated into QDs doped luminescent composites to improve their TC for its superior thermal-conductive ability and negligible absorption of visible light. However, because of the microscale diameter of hBN, there were considerable interfacial thermal resistance between fillers and between fillers and matrix, which made it inefficient to enhance TC. Considering light scattering effect of hBN may increase the probability that QDs reabsorb the light and be harmful to the luminous efficiency of luminescent composites, the hBN filling load was limited when they were used, resulting in a limited enhancement of TC[30]. To specifically display the superiority of radially aligned UPEF networks on the TC enhancement of QDs-polymer composites, the TC enhancement δ and TC enhancement efficiency η of the fillers have been calculated as the follow equation[33,36]:

$$\delta = TC/TC_0\ , \tag{1}$$

$$\eta = (TC - TC_0)/(100\varphi TC_0) \times 100\%\ , \tag{2}$$

where TC and TC_0 are the thermal conductivities of QDs-polymer composites with certain loading of fillers (UPEF and hBN) and polymer matrix, respectively. φ represents the loading fraction of fillers in the composites. The calculated results are listed in Table 1. It can be seen that the loading fraction of hBN is generally lower than 15 wt% considering their negative effects on light output. Therefore, the composites exhibited low TC (< 0.5 W m^{-1} K^{-1}) and η (< 35%) due to the enormous interfacial thermal resistance between the unconnected hBN platelets. In contrast, RA-PE with continuous and

long-range heat dissipation pathways showed superior characteristics of high TC with η of around 300%. This comparison demonstrated that radially aligned UPEF networks show superior ability to enhance thermal conductivity and potential to be used in the QDs-polymer composites for thermal management.

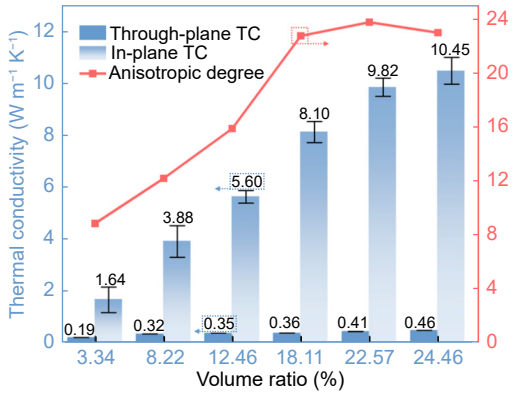

Fig. 4 | Through-plane TC, in-plane TC and anisotropic degree of TC of RA-PE with different UPEF volume ratio, respectively.

Figure 1(b) illustrates light conversion process within luminescent composites. QDs/phosphor absorb blue light and then emit red/yellow light. Due to the non-radiative process, heat generates during light conversion process which raises the temperature of illuminated QDs-polymer composites. Figure 1(c) gives the schematic of operated transmissive WLDs. A LD emits collimated blue laser beam which incidents downward onto the geometric center of QDs-polymer composites. Part of the incident blue light is absorbed by QDs/phosphor and converted to red/yellow light. Then, the unconverted blue light mixes with converted red and yellow light to form white light. In QDs-RAPE, massive UPEF are incorporated. The highly stretched UPEF contain polyethylene chains which transports phonon in a high speed[35,37]. Thanks to the radially aligned UPEF networks, QDs-RAPE can solve the thermal issue of WLDs of which heat is concentrated in the center of luminescent composites. According to Fig. 1(c), the generated heat in the center of QDs-RAPE could be radially dissipated by the UPEF networks, while the heat is aggregated in QDs-LC and forms high temperature. To study the temperature and heat flux distribution of QDs-LC and QDs-RAPE, finite element method (FEM) was utilized, as shown in Fig. 5. The related thermal parameters and boundary conditions are shown in Fig. S2. The heat source was located on the center to simulated the heat generation of WLDs. Under the same boundary condition of fixed temperatures, it can be seen that the radially aligned UPEF networks construct rapid heat transfer pathways to realize a much more uniform temperature distribution, while that of QDs-LC is concentrated in the center. Concretely, the heat flux in the UPEF is considerably higher than that in silicone, and it can be maintained along the whole radial direction due to the continuous UPEF. Additionally, the heat transfer mechanism of three-dimensional hBN network was investigated in our previously study[30]. We built interconnected thermal-conductive channels by contacting hBN platelets with each other to reduce interfacial thermal resistance. However, the huge interfacial thermal resistance between the contact hBN platelets were still non-negligible which created a break in the heat dissipation channels and destroyed the continuity of the heat flux. Thus, the continuous heat dissipation pathways in long-range built by UPEF was proved to be the key to the high thermal-conductive ability of QDs-RAPE.

Figure 6 compared the thermal performances of QDs-LC- and QDs-RAPE- converted WLDs from 300 to 1500 mA, under different UPEF volume ratio of 8.15, 11.93, 17.70, 21.92 and 26.70 vol%. The thermal conductivity of QDs-RAPE is nearly equal to RA-PE with the same UPEF volume fraction due to the small size and low volume fraction of phosphor (about 13 μm and 5 vol%) and QDs

Table 1 | Comparison of κ, δ and η of this work with previously reported related QDs-polymer composites.

Matrix	Filler	Loading fraction	Aligned architecture	κ (W m^{-1} K^{-1})	δ	η	Year
Silicone	hBN	2 vol%	None	$\kappa_{\perp}$ = 0.27	1.50	25.00%	2018[20]
Silicone	hBN	2 wt%	Vertically arranging	$\kappa_{\perp}$ = 0.17	1.23	11.43%	2020[27]
Silicone	hBN	15 wt%	None	$\kappa_{\perp}$ = 0.27	1.82	5.51%	2021[28]
Silicone	hBN	4.5 wt%	3D-interconnected	$\kappa_{\perp}$ = 0.37	2.49	33.19%	2022[30]
Silicone	hBN	10 wt%	3D-interconnected	$\kappa_{\perp}$ = 0.87	4.83	38.33%	2023[29]
Silicone	UPEF	3.34 vol%	Radially aligned	$\kappa_{//}$ = 1.64	10.93	297.41%	This work
Silicone	UPEF	8.22 vol%	Radially aligned	$\kappa_{//}$ = 3.88	25.86	302.67%	This work
Silicone	UPEF	24.46 vol%	Radially aligned	$\kappa_{//}$ = 10.45	69.66	280.83%	This work

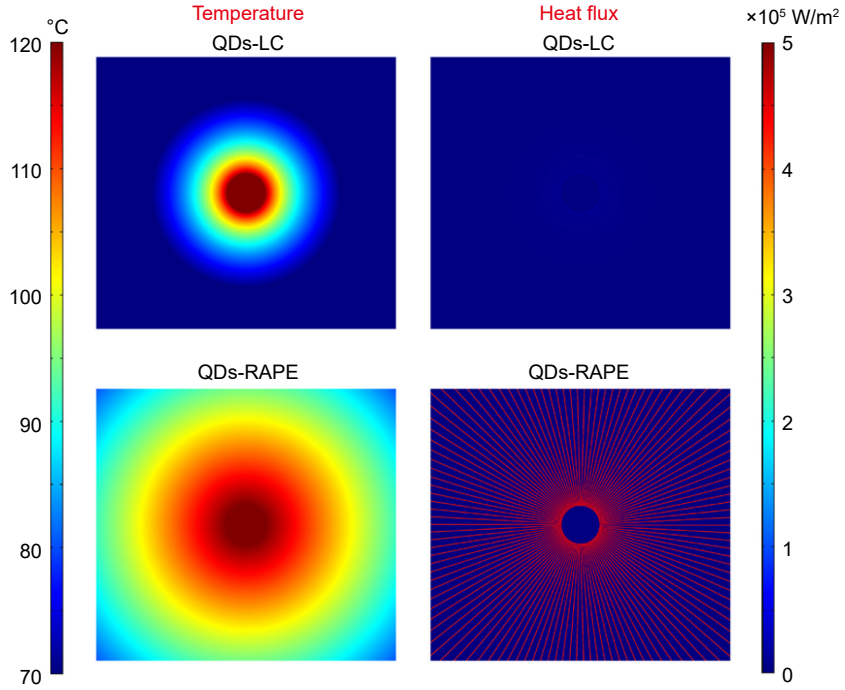

Fig. 5 | Simulated temperature and heat flux distribution of (**a**) QDs-LC and (**b**) QDs-RAPE.

(about 10 nm and 0.04 vol%), which is proved by calculation in supplementary information and the results are listed in Table S2. The composites were prepared by controlling the same mass of QDs-phosphor gel and embedding UPEF with different volume ratio. Surface temperature distributions of the WLDs under 700 and 1000 mA were measured by an infrared thermal imager, as illustrated in Fig. 6(a) and 6(b), respectively. Surface emissivity of the tested samples was set as 0.98, and the distance between samples and camera lens was set to 0.3 m, as shown in Fig. 6(c). It should be noted that the results were recorded after the temperature were stable. Figure S3 compares the heat power of the samples. The differences among QDs-LC and the QDs-RAPEs are small, and as the UPEF volume ratio increased, the heat power of QDs-RAPE increased slightly. Temperature distributions of QDs-LC, 8.15 and 26.70 vol% QDs-RAPE showed that the maximum surface temperature was located in the center of the samples, and that of QDs-RAPE was much more uniform than QDs-LC. Under driving current of 1000 mA, the maximum temperature of QDs-LC was 429 °C and the temperature gradient (listed in Table S3) along the radial direction was as high as 32146.4 K m^{-1}. Thanks to the marvelous heat dissipation ability of QDs-RAPE, the 8.15 vol% and 26.70 vol% QDs-RAPE showed much lower maximum surface temperatures of 86.5 and 68.8 °C, and much more uniform temperature distributions of temperature gradients of 4856 and 3224 K m^{-1} under 1000 mA, respectively. Compared with QDs-LC, 8.15 and 26.70 vol% QDs-RAPE reduced the maximum surface temperatures by 342.5 and 360.2 °C, and the temperature gradients by 84.9% and 90.0%, respectively. Figure 6(d) gives variation curve of maximum surface temperatures of different samples under increasing driving currents from 300 mA to 1500 mA. The temperature of QDs-LC was higher than QDs-RAPE under each driving current and the differences were enlarged as the driving currents increase. When the driving current reached 1000 mA, surface temperature of QDs-LC was too high, which caused thermal quenching. QDs-RAPE maintained much lower temperature from 300 mA to the maximum driving currents (1500 mA) of the blue-emissive laser diode, and temperatures were decreased as UPEF volume ratio increased. The results showed that QDs-RAPE owned superior cooling ability on the application of QDs-converted WLDs. The sharp reduction on the temperature of luminescent composites would be beneficial for the optical performances of QDs-converted WLDs.

Figure 7 shows optical performances of QDs-LC- and QDs-RAPE- converted WLDs. The samples were excited by blue laser diodes with a peak wavelength of 450 nm under different driving currents. Figure 7(a) displays spectra power distribution of QDs-LC, 8.15 and 21.92

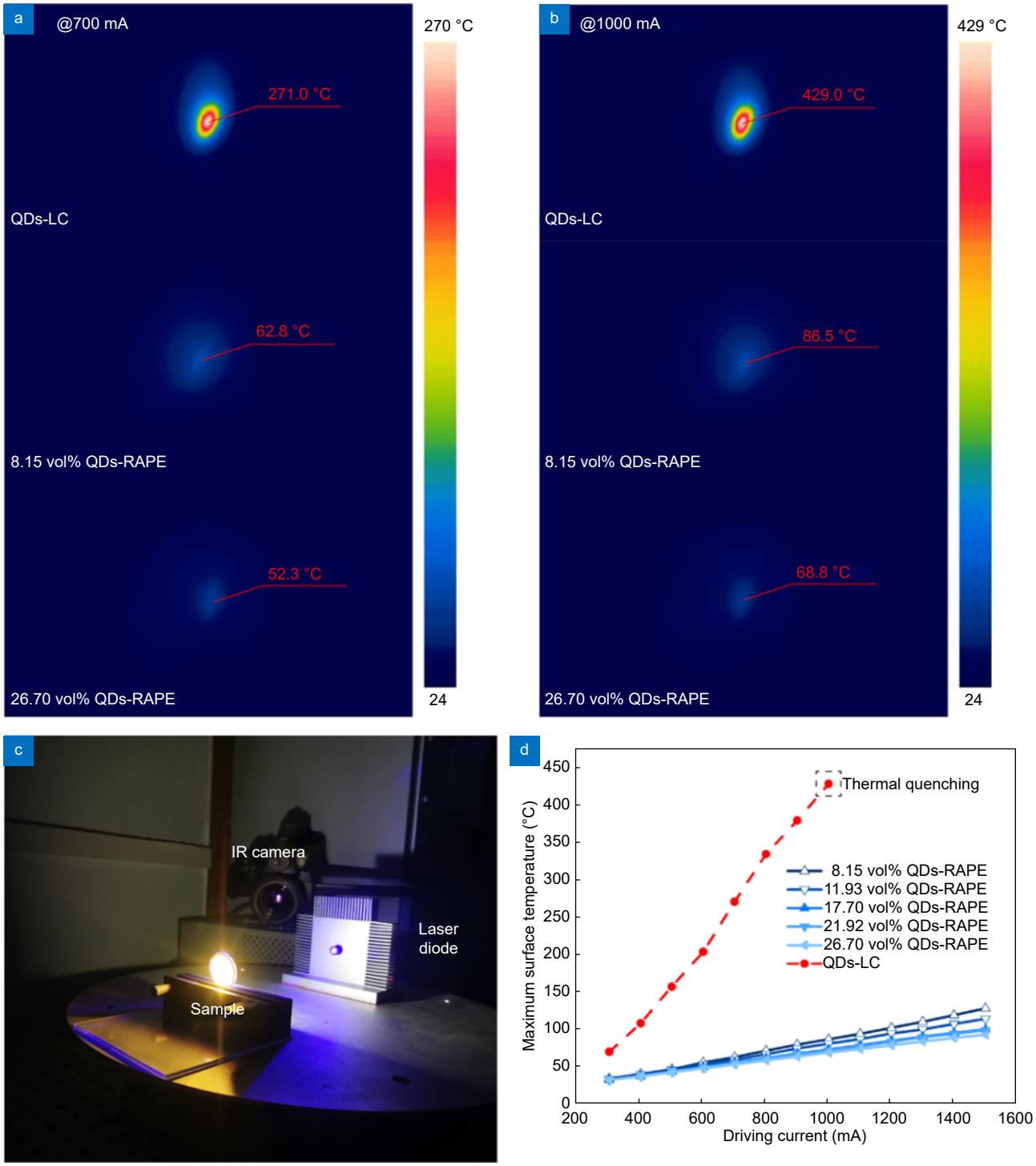

Fig. 6 | Surface temperature distributions of the three samples under driving currents of (**a**) 700 mA and (**b**) 1000 mA. (**c**) Temperature measurement setup. (**d**) Maximum surface temperature of the samples under different driving currents.

vol% QDs-RAPE under driving current of 700 mA, respectively. 8.15 and 21.92 vol% QDs-RAPE exhibited high LE of 155.85 and 127.92 lm W^{-1} as well as high CRI of 87.9 and 88.7. For QDs-LC, it had a LE of 134.04 lm W^{-1} and a lower CRI of 84.2. Meanwhile, CCT of QDs-RAPE of different UPEF volume ratio were around 4500 K, while that of QDs-LC was 8187 K. The above results indicated that adding radially aligned UPEF could be beneficial for the LE and CRI, and reduce the CCT of the WLDs. Under lower UPEF volume ratio, LE can be enhanced. Figure 7(b) displays the spectral power distribution of the QDs-RAPE-based WLDs under driving

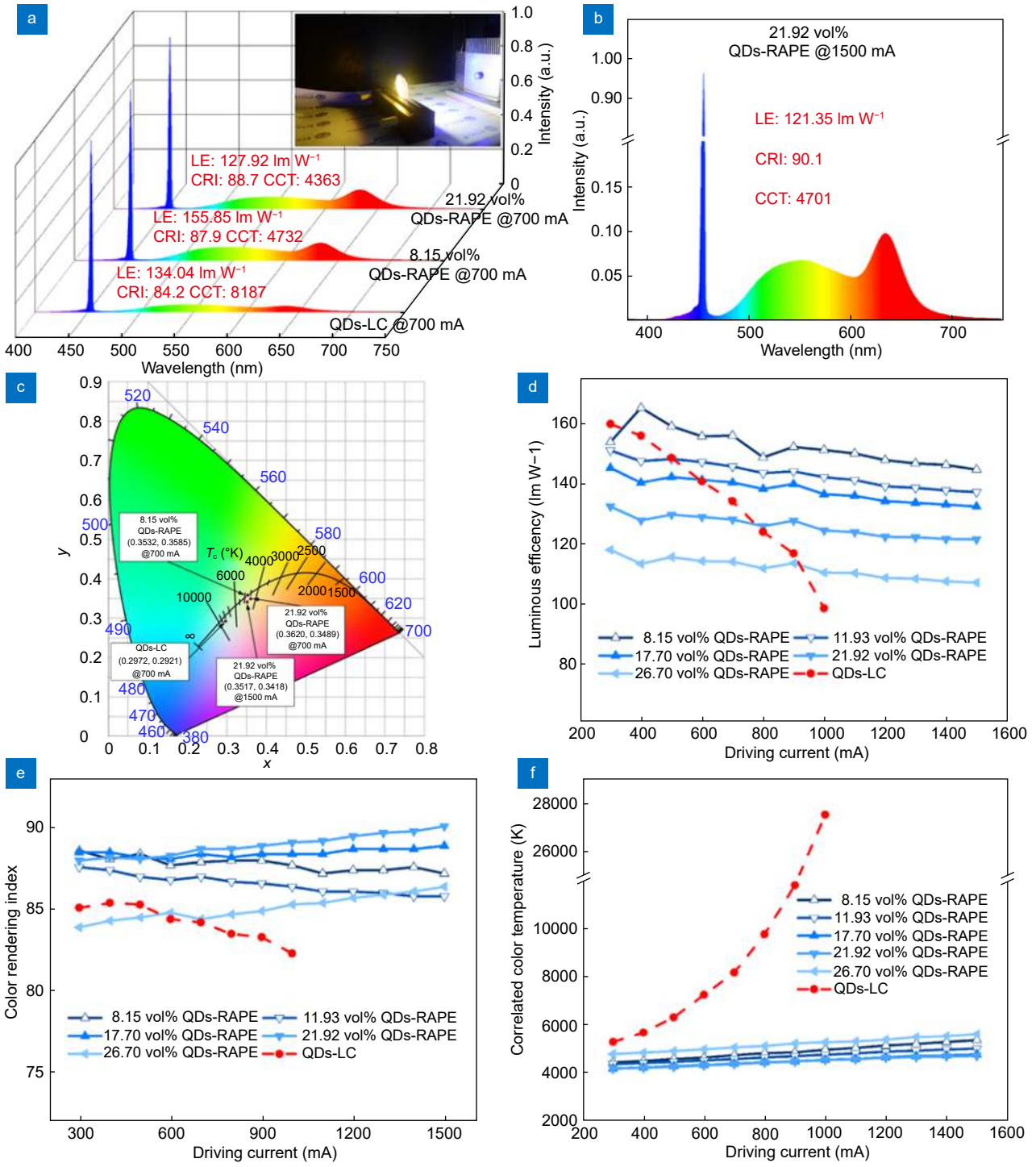

Fig. 7 | (**a**) Spectral power distributions and optical properties of QDs-LC, 8.15 vol% and 21.92 vol% QDs-RAPE under driving current of 700 mA. Inset is the photograph of QDs-RAPE with illumination. (**b**) Spectral power distribution and optical properties of 21.92 vol% QDs-RAPE under driving current of 1500 mA. (**c**) The coordinates of the luminescent composites in the CIE 1931 diagram. (**d**) LE, (**e**) CRI and (**f**) CCT of QDs-RAPE (8.15, 11.93, 17.70, 21.92 and 26.70 vol%) and QDs-LC under different driving currents from 300 to 1500 mA.

current of 1500 mA. It is seen that the CRI of 21.92 vol% QDs-RAPE reached as high as 90.1, representing its marvelous color rendering ability. Figure 7(c) illustrates the location of the WLDs in the CIE 1931 diagram. QDs-RAPE converted WLDs distributed near the central region of Planck blackbody curve, implying they were neutral white light with high quality. It can be seen from Fig. 7(d) that, LE of QDs-RAPE and QDs-LC was decreased

as the driving currents increased, which was attributed to the rising temperature. From 300 to 1000 mA, that the LE of QDs-LC decreased by 38.63%. Comparing to QDs-LC, LE of QDs-RAPE showed a more stable trend. It only slightly decreased from 300 to 1000 mA and the decrease was lower than 10% when driving currents reached 1500 mA. As the volume fraction of UPEF increased, Fig. 7(e) gives the variation of CRI under increasing driving currents. It is seen that CRI of QDs-LC was lower than 85, and decreased as the driving currents increased. In contrast, CRI of QDs-RAPE of different UPEF volume ratio were generally higher than QDs-LC, and it exceeded 90 with 21.92 vol% QDs-RAPE under 1500 mA. It is noting that under low UPEF volume ratio (8.15 and 11.93 vol%), CRI of QDs-RAPE decreased under the increasing driving currents, but the trend of CRI became opposite of the higher ones (17.70, 21.92 and 26.70 vol%). In addition, CCT of QDs-LC increased sharply from 5287 K to 27540 K as the driving currents increased, while that of QDs-RAPE were stable, which only variated in a small range of neutral white light (from 4000 K to 5500 K). In a word, QDs-RAPE-converted WLDs exhibited more superior and stable optical performances compared with QDs-LC.

To furtherly investigate the mechanism of optical performances improvement brought by radially aligned UPEF networks, enhancement ratio of yellow- and red- light intensity of QDs-RAPE to QDs-LC from 300 to 1000 mA were calculated, as shown in Fig. 8 and Table S4. Both enhancement ratio of yellow- and red-light intensity increased with increasing driving currents. This is mainly because that the much lower working temperature of QDs-RAPE strengthened the light-converted ability of QDs/phosphor particles under the same power as QDs-LC. Being attributed to the poorer thermal stability of QDs, enhancement ratios of red light were sharply higher than that of yellow light, implying that thermal management plays crucial role in high-performance lighting application of QDs. Moreover, adding UPEF with an average diameter of 20 μm helps reinforcing the light scattering effect, which may cause light loss in the luminescent composites. As UPEF volume ratio increased, enhancement ratio of yellow- and red- light intensity decreased, which was mainly due to the light loss from the enhanced light absorption of QDs caused by the scattering effect. Under lower driving currents, light loss brought by UPEF was stronger than light enhancement brought by temperature reduction, resulting in negative effect on the enhancement of light intensity. The enhancement ratio of yellow light was significantly dropped as UPEF volume ratio increased, while the drop was much smaller of red light. The dropped light intensity of QDs-RAPE under increasing UPEF volume ratio resulted in a decrease in LE. The above analysis indicated that overloading of UPEF is inadvisable and the volume fraction of UPEF should be controlled in a suitable range (8.15, 11.93 and 17.70 vol% in this work) to retain the optical performance. It can be concluded that, introducing radially aligned UPEF networks into QDs-polymer composites is conducive to optical performance of the corresponding WLDs due to its advanced cooling ability, especially under high power conditions.

Conclusion

QDs are usually embedded in polymer matrix with

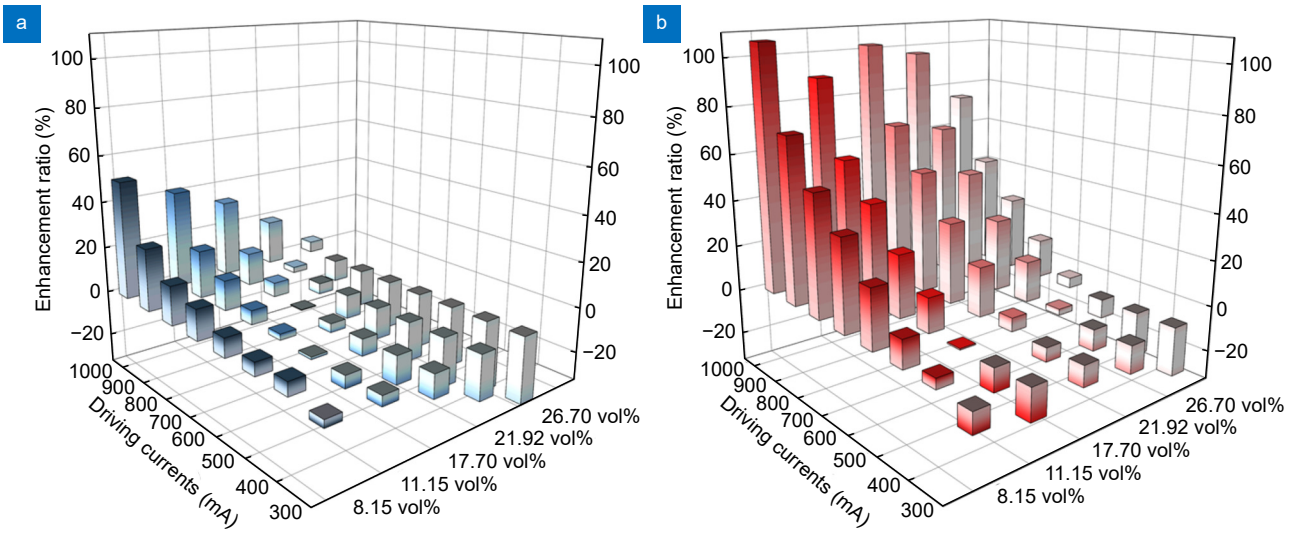

Fig. 8 | Enhancement ratios of (**a**) yellow- and (**b**) red- light intensity of QDs-RAPE to QDs-LC under different driving currents.

extremely low thermal conductivity which leads to severely thermal issues. Common solutions for QDs' thermal managements are based on incorporating microscale hBN fillers into the composites. However, due to the existing enormous interfacial thermal resistance, this strategy is inefficiency to transfer heat across a long distance. To solve this issue, we proposed to establish long-range radial heat dissipation pathways by establishing radially aligned UPEF networks in QDs-polymer composites. The composites of different volume ratio of UPEF (3.34, 8.22, 12.46, 18.11, 22.57 and 24.46 vol%) showed high thermal conductivity of exceeding 1.64 W m^{-1} K^{-1} and reached as high as 10.45 W m^{-1} K^{-1} of 24.46 vol%, which were 10.93 and 69.66 times that of pure silicone, respectively. Both thermal and optical performances of QDs-LC and QDs-RAPE were characterized. Under driving current of 1000 mA, QDs-RAPE of different UPEF volume ratio could realize much lower temperature over 342.5 °C than QDs-LC. Benefiting from the sharp temperature reduction, QDs-RAPE could stably operate under higher driving currents (1500 mA), while the QDs-LC suffered thermal quenching at 1000 mA. Under driving current of 700 mA, 8.15 vol% QDs-RAPE could achieve neutral white light with CCT of 4732K, LE of 155.85 lm W^{-1} and CRI of 87.9, while that of QDs-LC are 8187 K, 134.04 lm W^{-1} and 84.2, respectively. In addition, the CRI of 21.92 vol% QDs-RAPE could exceed 90 under driving current of 1500 mA to exhibit objects with true colors. The proposed strategy is promising for promoting the application of QDs in high-power optoelectronic areas.

References

1. Maheshwaran A, Bae H, Park J et al. Low-temperature cross-linkable hole transport materials for solution-processed quantum dot and organic light-emitting diodes with high efficiency and color purity. *ACS Appl Mater Interfaces* **15**, 45167–45176 (2023).
2. Zhang H Y, Wang B L, Niu Z J et al. Ultrasmall water-stable $CsPbBr_3$ quantum dots with high intensity blue emission enabled by zeolite confinement engineering. *Mater Horiz* **10**, 5079–5086 (2023).
3. Almeida G, van der Poll L, Evers WH et al. Size-dependent optical properties of InP colloidal quantum dots. *Nano Lett* **23**, 8697–8703 (2023).
4. Liao ZB, Mallem K, Prodanov MF et al. Ultralow roll-off quantum dot light-emitting diodes using engineered carrier injection layer. *Adv Mater* **35**, 2303950 (2023).
5. Ding SS, Steele JA, Chen P et al. Ligand‐mediated homojunction structure for high‐efficiency $FAPbI_3$ quantum dot solar cells. *Adv Energy Mater* **13**, 2301817 (2023).
6. Kong MQ, Osvet A, Barabash A et al. $AgIn_5S_8$/ZnS quantum dots for luminescent down-shifting and antireflective layer in enhancing photovoltaic performance. *ACS Appl Mater Interfaces* **115**, 52746–52753 (2023).
7. Zhang LX, Mei LY, Wang KY et al. Advances in the application of perovskite materials. *Nano-Micro Lett* **15**, 177 (2023).
8. Arya S, Jiang YR, Jung BK et al. Understanding colloidal quantum dot device characteristics with a physical model. *Nano Lett* **23**, 9943–9952 (2023).
9. Đorđević N, Schwanninger R, Yarema M et al. Metasurface colloidal quantum dot photodetectors. *ACS Photonics* **9**, 482–492 (2022).
10. Tian YY, Luo HQ, Chen MY et al. Mercury chalcogenide colloidal quantum dots for infrared photodetection: from synthesis to device applications. *Nanoscale* **15**, 6476–6504 (2023).
11. Wang YP, Yang YS, Zhang DK et al. Phosphorescent-dye-sensitized quantum-dot light-emitting diodes with 37% external quantum efficiency. *Adv Mater* **35**, 2306703 (2023).
12. Zhang DQ, Wei CT, Li XS et al. Highly solvent resistant small-molecule hole-transporting materials for efficient perovskite quantum dot light-emitting diodes. *ACS Appl Mater Interfaces* **15**, 44043–44053 (2023).
13. Kakuda M, Morais N, Kwoen J et al. Enhanced temperature stability of threshold current of InAs/GaAs quantum dot lasers by AlGaAs lateral potential barrier layers. *Opt Express* **31**, 31243–31252 (2023).
14. Yang T, Chen YH, Wang YC et al. Green vertical-cavity surface-emitting lasers based on InGaN quantum dots and short cavity. *Nano-Micro Lett* **15**, 223 (2023).
15. Jang HS, Yang H, Kim SW et al. White light-emitting diodes with excellent color rendering based on organically capped CdSe quantum dots and Sr_3SiO_5: Ce^{3+}, Li^+ phosphors. *Adv Mater* **20**, 2696–2702 (2008).
16. Yoon C, Yang KP, Kim J et al. Fabrication of highly transparent and luminescent quantum dot/polymer nanocomposite for light emitting diode using amphiphilic polymer-modified quantum dots. *Chem Eng J* **382**, 122792 (2020).
17. Chen KJ, Chen HC, Shih MH et al. The Influence of the thermal effect on CdSe/ZnS quantum dots in light-emitting diodes. *J Lightwave Technol* **30**, 2256–2261 (2012).
18. Woo JY, Kim KN, Jeong S et al. Thermal behavior of a quantum dot nanocomposite as a color converting material and its application to white LED. *Nanotechnology* **21**, 495704 (2010).
19. Zhao YM, Riemersma C, Pietra F et al. High-temperature luminescence quenching of colloidal quantum dots. *ACS Nano* **6**, 9058–9067 (2012).
20. Xie B, Liu HC, Hu R et al. Targeting cooling for quantum dots in white QDs-LEDs by hexagonal boron nitride platelets with electrostatic bonding. *Adv Funct Mater* **28**, 1801407 (2018).
21. Chang H, Zhong YC, Dong HX et al. Ultrastable low-cost colloidal quantum dot microlasers of operative temperature up to 450 K. *Light Sci Appl* **10**, 60 (2021).
22. Moon H, Lee C, Lee W et al. Stability of quantum dots, quantum dot films, and quantum dot light-emitting diodes for display applications. *Adv Mater* **31**, 1804294 (2019).
23. Li ZT, Li JX, Li JS et al. Thermal impact of LED chips on quantum dots in remote-chip and on-chip packaging structures. *IEEE Trans Electron Dev* **66**, 4817–4822 (2019).
24. Zheng H, Lei X, Cheng T et al. Enhancing the thermal dissipation of a light-converting composite for quantum dot-based white

light-emitting diodes through electrospinning nanofibers. *Nanotechnology* **28**, 265204 (2017).
25. Xu J, Hu BF, Xu C et al. A unique color converter geometry for laser-driven white lighting. *Opt Mater* **86**, 286–290 (2018).
26. Zheng F, Yang BB, Cao PY et al. A novel bulk phosphor for white LDs: $CsPbBr_3/Cs_4PbBr_6$ composite quantum dots-embedded borosilicate glass with high PLQY and excellent stability. *J Alloys Compd* **818**, 153307 (2020).
27. Zhou SL, Ma YP, Zhang XF et al. White-light-emitting diodes from directional heat-conducting hexagonal boron nitride quantum dots. *ACS Appl Nano Mater* **3**, 814–819 (2020).
28. Yang X, Zhou SL, Xie B et al. Enhancing heat dissipation of quantum dots in high-power white LEDs by thermally conductive composites annular fins. *IEEE Electron Device Lett* **42**, 1204–1207 (2021).
29. Zhao WX, Xie B, Peng Y et al. Cooling photoluminescent phosphors in laser-excited white lighting with three-dimensional boron nitride networks. *Opt Laser Technol* **157**, 108689 (2023).
30. Xie B, Wang YJ, Liu HC et al. Targeting cooling for quantum dots by 57.3°C with air-bubbles-assembled three-dimensional hexagonal boron nitride heat dissipation networks. *Chem Eng J* **427**, 130958 (2022).
31. Xie YY, Yang DD, Zhang LL et al. Highly efficient and thermally stable QD-LEDs based on quantum dots-SiO_2-BN nanoplate assemblies. *ACS Appl Mater Interfaces* **12**, 1539–1548 (2020).
32. Zhang LL, Xie YY, Tian ZZ et al. Thermal conductive encapsulation enables stable high-power perovskite-converted light-emitting diodes. *ACS Appl Mater Interfaces* **13**, 30076–30085 (2021).
33. Wang XW, Wu PY. 3D vertically aligned BNNs network with long-range continuous channels for achieving a highly thermally conductive composite. *ACS Appl Mater Interfaces* **11**, 28943–28952 (2019).
34. Xu YF, Kraemer D, Song B et al. Nanostructured polymer films with metal-like thermal conductivity. *Nat Commun* **10**, 1771 (2019).
35. Wang XJ, Kaviany M, Huang BL. Phonon coupling and transport in individual polyethylene chains: a comparison study with the bulk crystal. *Nanoscale* **9**, 18022–18031 (2017).
36. Xie B, Zhao WX, Luo XB et al. Alignment engineering in thermal materials. *Mater Sci Eng R Rep* **154**, 100738 (2023).
37. Henry A, Chen G. Anomalous heat conduction in polyethylene chains: theory and molecular dynamics simulations. *Phys Rev B* **79**, 144305 (2009).

Acknowledgements

This work is supported by the National Natural Science Foundation of China (52106089).

Competing interests

The authors declare no competing financial interests.

Supplementary information

Supplementary information for this paper is available at https://doi.org/10.29026/oea.2024.240036

Scan for Article PDF